

Applications of synchrotron-based micro-imaging techniques to the chemical analysis of ancient paintings†‡

Marine Cotte,^{*ab} Jean Susini,^b V. Armando Solé,^b Yoko Taniguchi,^c Javier Chillida,^d Emilie Checroun^e and Philippe Walter^a

Received 25th January 2008, Accepted 20th March 2008

First published as an Advance Article on the web 22nd April 2008

DOI: 10.1039/b801358f

Ancient paintings are complex materials in terms of chemical analysis because they are usually made of organic/mineral, amorphous/crystallized, major/minor mixtures, evolving with time, and organized in micrometric multi-layered arrangements. In this context, synchrotron micro-imaging techniques offer a powerful analytical platform to reveal the two dimensional atomic, molecular and structural compositions of such complex systems, at a micrometre resolution. The two selected examples illustrate the two main concerns of restorers and conservators: looking backwards, to get insight into ancient artistic practices (in particular through the identification of pigments and binders in Bamiyan Buddhist mural paintings); and looking forward, to preserve works of art as long as possible (through a better understanding of cinnabar blackening in Medieval Spanish paintings). From the analytical chemistry point of view, they also illustrate the relevance of combining micro X-ray fluorescence, micro X-ray absorption spectroscopy, micro X-ray diffraction, and micro-FTIR for the complete analysis of painting cross-sections (binders and pigments).

Introduction

Chemical analyses carried out on ancient paintings are usually devoted to two main objectives. On one hand, they intend to understand the painter techniques (choice of pigments, of binders, mixtures, applications *etc.*); it can for example enable the following of painting evolutions, such as pigments synthesis across centuries; or to date a painting, thanks to the identification of constitutive pigments. On the other hand, some analyses focus on the better understanding of alteration mechanisms (pigment whitening or blackening, apparition of cracks, of efflorescence *etc.*). In this case, the attention is paid less to the past of the painting than to its future.

The analysis of major elements is generally the first step to identify pigments. For example, in a red pigment, mercury is associated to mercury sulfide, HgS (natural cinnabar, or synthetic vermilion) and lead to minium (Pb₃O₄). Arsenic is associated to orpiment (As₂S₃) in yellow pigment and to realgar (AsS) in a red pigment.¹ This basic identification is traditionally

carried out by X-ray fluorescence using various exciting probes (electrons, X-rays, ions). In addition, the analysis of minor or trace elements can provide supplementary information. For example, the presence of Mg, Cl, K, or Ca enables the distinction between natural ultramarine and synthetic pure lazurite.² However, these identifications become much trickier when the pigment is made of several metals, or in the case of mixtures of pigments. The phase identification, usually performed by X-ray diffraction (XRD) or by Raman spectrometry, can be very useful to complete the elemental analysis. Some pigments show a clear evolution across decades and can be used to date paintings. For instance, the different lead-yellow pigments containing tin and/or antimony seem to be temporally and geographically specific indicators in the Mid-European paintings, from the 15th to the 19th century.³ Similarly, the two phases of titanium dioxide, anatase and rutile, are sometimes used as chronological references for modern paintings, as their synthesis and trade correspond to two different periods of the 20th century (around 1920 and 1940, respectively).⁴ However, such a dating procedure can be hampered by the parallel use of natural titanium dioxides, occurring since antiquity.⁵ Chromatographic techniques are usually favoured for the analysis of binders, as they give detailed identification of organic ingredients. Recently, Fourier transform infrared spectroscopy (FTIR) and secondary ion mass spectrometry (SIMS) demonstrated the relevance of imaging techniques providing 2D information. They also have the unique asset to give access to both organic and inorganic materials, as well as their interaction products.⁶

In parallel to these laboratory techniques, the art and archaeology communities show a growing interest for synchrotron radiation, as shown by the increasing number of dedicated workshops and conferences.⁷ Application of micro-imaging techniques is particularly relevant for the study of ancient

^aCentre of Research and Restoration of the French Museums - UMR171 CNRS, Palais du Louvre, 14 quai F. Mitterrand, Paris, 75001, France. E-mail: marine.cotte@culture.gouv.fr

^bEuropean Synchrotron Radiation Facility, BP-220, Grenoble Cedex, 38043, France

^cJapan Center for International Cooperation in Conservation- National Research Institute for Cultural Properties, Tokyo, 13-43, Ueno koen, Tokyo, 110-8713, Japan

^dPainting restorer, Barcelona, Spain

^ePainting restorer, Paris, France

† This paper is part of a JAAS themed issue on Synchrotron Radiation, with guest editors Alex von Bohlen and Metin Tolan.

‡ Electronic supplementary information (ESI) available: Stratigraphy of the paint structure of Foladi Cave 4 (sample FDM55), from μ FTIR, μ XRF, μ XRD analyses. See DOI: 10.1039/b801358f

paintings, regarding their micrometric multi-layered arrangement, and their chemical complexity (mixture of inorganic minerals and organic binders, crystallized and amorphous phases, major and minor elements). Four different imaging techniques are illustrated in this paper: micro X-ray fluorescence (μ XRF), micro X-ray diffraction (μ XRD), micro-FTIR spectroscopy (μ FTIR), and micro X-ray absorption near edge spectroscopy (μ XANES).

These four techniques benefit from the source brightness which enables the beam size to be focussed close to the diffraction limit (a few microns for mid-infrared, down to submicron for X-rays), without compromising the flux. Hence the possibility to acquire signal on a reduced pixel size with a reduced dwell time (from tens of second for μ FTIR to less than one second for μ XRF or μ XRD). The combination of these two aspects is essential while acquiring high resolution 2D-mappings. Corollary, the detection limit is directly correlated to the signal to noise ratio (S/N). Minor and trace elements or phases can be identified with synchrotron equipment when classical lab instruments may not be sensitive enough to detect them. In addition to its brightness, the synchrotron source provides a broad band spectrum, from infrared to X-rays, allowing micro-spectroscopies in various energy ranges.

Finally, an intrinsic benefit of the synchrotron facility is the diversity of available techniques. Each technique is, in itself, very powerful, but their combination is a major asset, in particular when studying complex systems such as ancient paintings. At the ESRF for example, micro-imaging beamlines ID21, ID22 and ID18F offer locally multi-modal microscopes.

Following some practical considerations about sample preparations and experimental set-ups, two examples are developed hereafter. In the first one, studies are carried out on paintings from the Monastery of Pedralbes (14th century), Barcelona, Spain. Under an ancient whitewash, restorers revealed the original gothic painting which was highly damaged. In particular, the whole background, made of cinnabar, a red mercury sulfide pigment, had turned grey. In the context of previous analyses of similar cases,^{8–10} chlorine was suspected to play a role in the blackening process. To check its presence and its potential interaction with cinnabar, μ XRF and μ XANES analyses were carried out at both chlorine and sulfur K-edges. In the second example, analyses intended to reveal Bamiyan Buddhist painting practices (5th to 9th century). In order to identify both organic binders and mineral-based inorganic pigments, painting fragments were submitted to a multi-modal approach, combining μ XRF, μ XRD and μ FTIR.

Experimental

Instrumental set-up and sample preparation

The traditional preparation of painting stratigraphies consists of polished cross-sections of a fragment of painting embedded in resin. This method offers a handy object, that can be easily observed under visible as well as an electron microscope. Some analytical techniques (FTIR, SIMS, SEM *etc.*) require a more careful preparation as the data quality is primarily determined by the surface quality, hence dedicated developments aimed at improving surface preparation.^{11,12} When dealing with

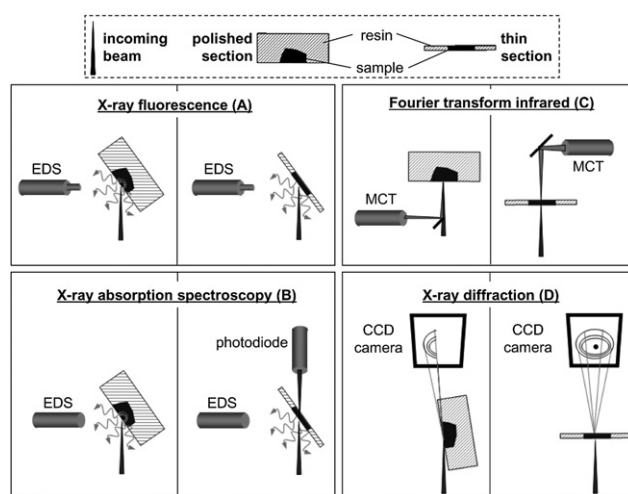


Fig. 1 Sketches of the different set-ups for μ XRF (A), μ XANES (B), μ FTIR (C) and μ XRD (D). For each technique, the set-up is displayed with a massive polished section, in “reflection” mode (left) and with a thin section, in “transmission” mode (right).

synchrotron-based micro-imaging, it is a conventional preparation when experiments can be performed in “reflection” mode: measuring the light emitted (XRF, XANES) (Fig 1A,B), reflected (infrared) (Fig. 1C) or diffracted (XRD) (Fig. 1D) on the surface of a bulky sample. This kind of set-up can also be used when working on whole museum objects.

However, in certain circumstances, it can be highly useful to work on thin sections instead of polished sections. This preparation is much more difficult because if the painting fragment is too fragile, it will explode, leaving an empty hole. The presence of organic binders in the painting strongly increases the success of this operation.

Yet, it can be worth facing these technical hitches considering the improvements gained in terms of data acquisition. For XRD (Fig. 1D), the sample orientation is no longer fixed to an almost grazing incidence ($\sim 20^\circ$). Instead, the sample can be turned in respect to the beam. In this configuration, the beam projection on the sample surface is much smaller, and the positioning easier. Besides, the data quality is highly improved as this geometry enables the complete collection of the diffracted beam, while, in reflection mode, almost half of the ring is in the shadow of the object. This is particularly important for the smallest rings that may be completely hidden in the reflection mode. In the example presented hereafter, several sections were prepared with thickness ranging from 5 to 200 μ m. Analyses were mainly performed on sections 30 μ m-thick, giving a good trade off between transmission and absorption.

For FTIR, geometry is unchanged when working in “reflection” or “transmission” mode, the sample always being placed perpendicular to the beam (Fig 1C). The signal quality is much higher when measuring in transmission rather than reflection but it implies the preparation of appropriate sections. Indeed, too thick sections will lead to the complete absorption of the signal. For paintings, the ad-hoc thickness is between 2 to 5 μ m, depending on the mineral charge. The main drawback, which exists when working with both polished and thin sections, is the possible interference of the embedding resin in the infrared

spectra. When the interest of FTIR analyses is focussed on identification of organic materials, an alternative preparation consists of placing a piece of sample into two diamond windows, with the stratigraphy perpendicular to the windows and pressing (*cf.* visible picture in Fig. 7). It leads, inevitably, to some distortion inside the sample structure, but offers a sample free of any contamination.

For XRF analyses (Fig. 1A), a thin section is usually better suited to avoid in-depth structure averaging which spoils the lateral resolution. When the sample is sufficiently homogeneous along the beam direction, or when working at low energy, polished sections are favoured. This set-up was used to study Spanish paintings at the sulfur and chlorine K-edges. Conversely, when working at high energy, preparing thin sections (<10 μm) limits contribution from the bulk.

XANES analyses exhibit similar assets. Besides, spectra can be simultaneously measured in transmission, with a better signal to noise ratio than in fluorescence if the element of interest is sufficiently concentrated. This approach is particularly relevant when radiation damage is a critical issue. Indeed, if the sample is radiation sensitive, as may happen with ancient biological/organic matter (tissue, blood, copper carboxylates *etc.*), reduction of the dwell time has to be considered. In these conditions, absorption geometry with a photodiode downstream to the sample can offer better detection efficiency than X-ray fluorescence geometry using an X-ray dispersive detector which usually has a very low collection aperture and limited counting rate.

As illustrated hereafter, combining several methods offers a wider and more detailed view of the object than the distinct point of view brought by a single technique. When possible, it is worthwhile to carry out different analyses on the same section. This approach is rather natural when combining different X-ray techniques. Indeed, several analyses (XRF/XRD or XRF/XANES) can be performed simultaneously, with a single microscope. The combination X-ray/FTIR is technically more challenging. With some possible compromises on data quality, X-ray and infrared analyses can be performed on the same samples, as it was done on the patina of African statues.¹³ For the study of Bamiyan paintings, it was preferred to adapt sample preparation specifically to each microscope. With the aim of carefully studying organic binders present in painting by μFTIR , micro-compression was favoured to microtome as it shelters from any spectra contamination by embedding material. For $\mu\text{XRF}/\mu\text{XRD}$, the presence of embedding resin was not an inconvenience; hence studies were performed on thin sections about 30 μm -thick obtained with a microtome. Analysis of cinnabar paintings was conducted on polished section.

Instruments

Micro XRF/XANES at low energies. Cinnabar paintings were studied at the X-ray microscopy beamline, ID21, at the ESRF (Grenoble, France) (www.esrf.fr/UsersAndScience/Experiments/Imaging/ID21).¹⁴ The scanning X-ray microscope is optimized for very low background and low detection limits and can be operated in air or under vacuum. The energy range goes from 2.1 to 7.2 keV. Here, XRF and XANES were performed at the sulfur and the chlorine K-edges (2.5 and 2.9 keV, respectively). A

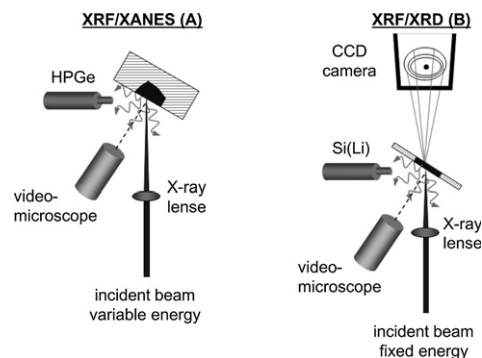


Fig. 2 The set-up used for the analysis of painting. (A) $\mu\text{XRF}/\mu\text{XANES}$ on polished sections of Pedralbes paintings; (B) $\mu\text{XRF}/\mu\text{XRD}$ on thin sections of Bamiyan paintings.

fixed-exit, double crystal Si (111) monochromator, located upstream of the microscope, determines the energy beam with a resolution of $\Delta E/E = 10^{-4}$ (corresponding to 0.3 eV at the considered energies). The beam size was reduced to $\sim 0.8 \times 0.2 \mu\text{m}^2$ (hor. \times ver.) thanks to Fresnel zone plates by geometrical demagnification of the synchrotron source. For μXANES , the probe pointing was stabilized down 0.5 μm .¹⁵ The micro fluorescence signal is collected in the horizontal plane perpendicular to the incident beam direction by using an HPGe solid-state, energy-dispersive detector (Fig. 2A).

Micro XRF/XRD at high energies. Synchrotron-based micro X-ray diffraction and micro X-ray fluorescence were performed at the beamline ID18F, at the ESRF (Grenoble, France) (www.esrf.fr/UsersAndScience/Experiments/Imaging/ID18F).¹⁶ This beamline is a high-energy multi-technique X-ray microscope. The double crystal monochromator, equipped with both Si [111] and Si [311] crystals, offers a wide energy range (6–70 keV) for optimal excitation conditions of a broad range of elements. In this experiment, the excitation energy was fixed at 28 keV and the beam was focussed to $15 \times 1 \mu\text{m}^2$ (hor. \times ver.). A CCD camera was used to collect X-ray diffraction patterns, in transmission. The fluorescence signal was collected simultaneously in the horizontal plane perpendicular to the incident beam direction with a Si(Li) energy-dispersive detector (Fig. 2B).

For all X-ray analyses (ID21 and ID18F), samples are mounted vertically, oriented with an angle of about 60° with respect to the incident beam (Fig. 2). They are raster-scanned horizontally and vertically to obtain two dimensional images. Cross-section stratigraphies are oriented horizontally in order that the best resolution of the beam (1 μm at ID18F, 0.2 μm at ID21) fits with the axis of the samples heterogeneity, whereas the average in the horizontal direction (15 μm at ID18F, 0.8 μm at ID21) is made over a rather homogeneous layer. A video-microscope, placed perpendicular to the sample, enables the observation of the sample under visible light, and the selection of region of interest.

Micro-FTIR. Micro infrared spectroscopy was performed with a Nicolet Continuum microscope coupled to a Nexus spectrometer, at the ID21 FTIR end-station (www.esrf.fr/UsersAndScience/Experiments/Imaging/ID21).¹⁷ Over the set of

analyses performed, aperture was tuned from $12 \times 12 \mu\text{m}^2$ to $8 \times 8 \mu\text{m}^2$. In the example given hereafter, lateral resolution was set to $12 \times 12 \mu\text{m}^2$ in order to keep a high flux all over the infrared domain ($4000\text{--}700 \text{ cm}^{-1}$), to spend a minimum of time in each pixel: 25 scans were sufficient to get a very good S/N in only 6 s.

Data treatment

X-Ray fluorescence spectra were fitted with PyMCA.¹⁸ This software is freely downloadable and allows interactive as well as batch processing of large data sets. It implements Levenberg–Marquardt and linear fitting algorithms to fit the spectra with constraints on the fitting parameters (detector characteristics, detection geometry, matrix composition, exciting beam, *etc.*). A complete emission line series (*i.e.*, M or L series) is fitted by taking into account theoretical intensity ratios and line emission energies. An example of fit is given in Fig. 3. In the present case, such a fit was essential to differentiate the M-lines emission of mercury from the K-lines of sulfur. While this code was originally developed to analyse fluorescence spectra recorded at synchrotron beam lines, an update was made towards laboratory instruments by implementing new options to simplify the analysis of spectra obtained with X-ray tubes. Fits were performed for each of the fluorescence spectra obtained on each pixel of 2D mappings, in batch processing, to produce elemental mappings.

For the treatment of X-ray diffraction data, the Debye–Scherrer diffraction rings are unwrapped and integrated *versus* the azimuthal angle to produce a 1D diffraction pattern thanks

to the ESRF package Fit2D.¹⁹ The set of data thus generated has a format similar to the fluorescence data, with, for each pixel, a 1D diffraction pattern.

Besides the treatment of fluorescence data, the PyMCA imaging capabilities allow a fast and interactive treatment of various spectral data through a purely graphical interface. This is particularly interesting in the presented studies because it allows a convenient combination of the different techniques (FTIR, XRF, and XRD). In the case of a combined acquisition of XRF and XRD data, one typical use is the generation of the 2D map of a certain element and the use of that map to find the different phases associated to the distribution of that element in the sample. Another possibility is to generate the 2D map associated to a particular diffraction angle and to use that map to generate the associated fluorescence spectra. Since the datasets of the different techniques are simultaneously handled, the scientist can go back and forth in the procedure while comparing the generated maps and taking maximum profit of the techniques cross-fertilization.

Results and discussion

Combination of micro X-ray fluorescence and micro X-ray absorption spectroscopy for the study of cinnabar blackening

The monastery of Pedralbes, Barcelona, Spain, was founded in 1326 by Queen Elisenda de Montcada, who lived there in seclusion after the death of her husband, King James II. The Queen was buried in the Gothic church of the monastery, in a highly decorated tomb. In a later period, due to either new fashion or painting alteration, it was decided to cover the walls with plaster (made of gypsum), producing a new, clean white background. Later on, this whitewash was partially and aggressively removed. At some places, the excessive removal led to some destruction of the gothic painting, and at other places, the incomplete removal left traces of gypsum. In 2007, the restoration of the grave was initiated for the gothic painting to be visible again. On the background wall, a beautiful but damaged polychromic flowered decoration appeared under the residual whitewash. These motifs were found to be drawn over a homogeneous dark-red layer. This background was red underneath, but unfortunately, highly altered on its surface. It was almost fully covered with a grey black superficial layer, strongly affecting its original aspect.

Chemical analyses were conducted to identify both the original pigment and the alteration products. Mercury and sulfur were easily identified by SEM-EDX (results not shown), demonstrating that the pigment was cinnabar, mercury sulfide (HgS), a deep red pigment, extensively used since antiquity. The identification of the alteration products was much more intricate, the altered layer being sometimes less than $5 \mu\text{m}$. The transformation into metacinnabar has long been a classical explanation for cinnabar blackening,²⁰ yet recent studies revealed that chlorine could play a role in cinnabar alteration processes.^{8–10} μXRF and μXANES analyses were carried out at chlorine and sulfur K-edges in order to assess the presence of chlorine and mercury-chloride compounds in the various layers of the painting.

Eight fragments were taken in different places of the monastery, exhibiting various degrees of darkening, ranging from

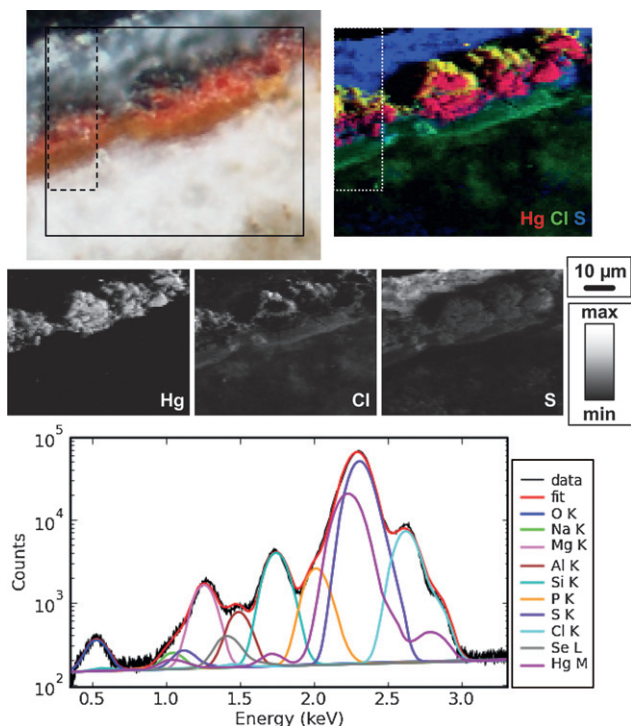


Fig. 3 Visible light picture of the polished section of painting from Pedralbes. The black rectangles indicate the areas analyzed by μXRF : fluorescence maps of Hg, S, Cl in RGB and grey level visualizations. Map size: $100 \times 80 \mu\text{m}^2$, step size: $1 \mu\text{m}$ in both directions. X-ray fluorescence spectrum, acquired at the Cl K-edge and fitted with PyMCA.

unaltered red to dark grey, including light grey. Visible and chemical observations showed that most of these fragments presented a superposition of red, black and white layers, successively. The thickness of the white translucent layer is mainly responsible for the different grey shades. The example presented here corresponds to the case of an extreme alteration (darker fragment), and gives a clearer vision of the chemical degradation.

Chemical mappings were first acquired with an excitation energy of 2.9 keV, above the chlorine K-edge. Fluorescence spectra show that sulfur and mercury are indeed the major elements, but interestingly, they are not systematically co-located (Fig. 3). They share the same distribution on red grains, corresponding to remaining cinnabar pigment that can be seen under visible light. Sulfur is also found in a concentrated state in a thick layer of about 10 to 20 μm , on top of the painting. This layer corresponds to the white translucent film covering the fragment. Looking more carefully, a thin layer of less than 5 μm can be observed covering the cinnabar grains, with mercury but without sulfur.

In the RGB coded image (Fig. 3), mercury and chlorine are plotted in red and green, respectively, therefore their co-location appears as a yellow layer. Chlorine is detected in two distinct regions: first, it is co-located with mercury in a black, thin layer (yellow on RGB display) embedding the red cinnabar grains. Second, it is also present in the under mercury-free layer, below the cinnabar grains.

In summary, in the different layers, three main elements, sulfur, mercury and cinnabar, are present, alone or co-located. To go beyond this simple elemental identification, μXANES was performed at the chlorine and sulfur K-edge in order to distinguish a simple co-location of elements from a real chemical complex. The fact that co-locations (Hg-S, Hg-Cl) change across the sample, lets assume a variety of sulfur and chlorine speciations in the different layers.

A more detailed map was acquired at 2.85 keV around this interfacial region, with a 0.5 μm step in both directions (Fig. 4 and Fig. 6A). As observed in Fig. 3, sulfur is concentrated on the top-layer, then absent in a very thin layer and then present at a lower extent, in association with mercury. Chlorine is concentrated on the surface of mercury grains, and diluted below

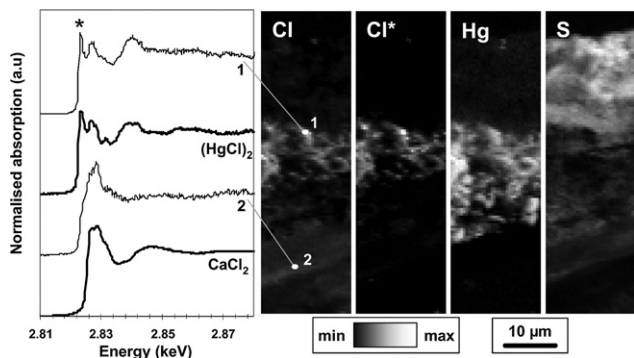


Fig. 4 X-Ray absorption spectra at the Cl K-edge: model compounds (calomel (HgCl_2) and calcium chloride (CaCl_2) and 2 spectra acquired on point #1 and #2. Elemental and chemical mappings, obtained at 2.8500 keV for Cl, Hg and S, and at 2.8231 keV for Cl^* . Map size: $60 \times 18 \mu\text{m}^2$, step size: 0.5 μm in both directions. Cf. visible picture in Fig. 3.

them. XANES spectra were acquired in these two domains at the Cl K-edge (2.795 to 2.895 keV). They clearly demonstrate that chlorine speciation is changing over the sample. Two characteristic spectra are displayed in Fig. 4. Spectra were fitted as a linear combination of various chlorine reference spectra (NaCl , KCl , CaCl_2 , MnCl_2 , calomel (HgCl_2), HgCl_2 , corderoite ($\text{Hg}_3\text{S}_2\text{Cl}_2$), egglestonite ($\text{Hg}_6\text{Cl}_3\text{O}(\text{OH})$), terlinguaite (Hg_2ClO)). Principles of the calculation and reference spectra can be found elsewhere.¹⁰ For each spectrum plotted in Fig. 4, the main component has been superimposed ($(\text{HgCl})_2$ for point #1 and CaCl_2 for point #2). Even if the distinction inside the different mercury–chloride phases is tricky, XANES offers a powerful tool to identify “Hg–Cl” bonding. Indeed, the various mercury chloride compounds exhibit a clear signature at 2.823 keV, which enables to easily distinguish them from the different alkaline and alkaline-earth chlorides. Chemical mapping of mercury chlorides was therefore performed by acquiring fluorescence with an excitation beam of 2.8231 keV (indicated as a star in Fig. 4). The corresponding chlorine map (Cl^* in Fig. 4) shows specific distribution of mercury chloride compounds. It confirms the different states of chlorine across the sample: chlorine is indeed chemically linked to mercury on the surface of cinnabar grains, whereas, below cinnabar, a form similar to CaCl_2 is suspected. In the present configuration, the beam energy was tuned to prevent calcium X-ray fluorescence. Yet, preliminary SEM analyses clearly showed its presence in the subjacent white mortar.

A comparable work was conducted at the sulfur K-edge to check the sulfur speciation in red, black and white regions. XANES spectra were first acquired across the sample, in the different characteristic layers. Fig. 5 highlights the main tendencies observed with three illustrative spectra. Point #1 was acquired on a red grain; it perfectly fits cinnabar feature. Point #2 was acquired in the grey layer covering cinnabar, in an area where Hg, Cl and S are present altogether. A small shift of the energy edge, from 2.4716 keV (point #1) to 2.4725 keV (point #2), confirms the presence of corderoite ($\text{Hg}_3\text{S}_2\text{Cl}_2$). Finally, the spectrum obtained at point #3 is characteristic of a sulfate, with an intense white line at 2.4828 keV. The spectrum of gypsum ($\text{CaSO}_4 \cdot 2\text{H}_2\text{O}$) is superimposed for comparison.

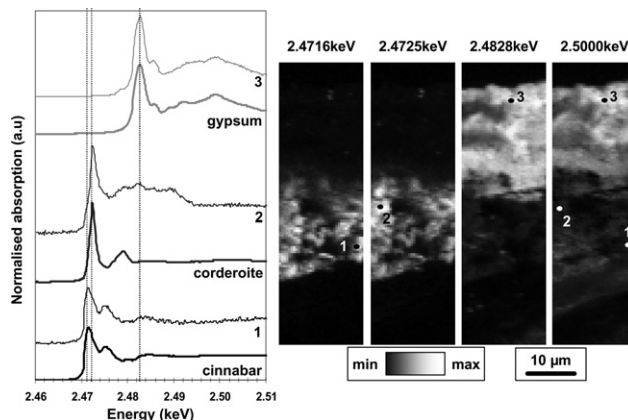


Fig. 5 X-Ray absorption spectra at the S K-edge: model compounds (cinnabar (HgS), corderoite ($\text{Hg}_3\text{S}_2\text{Cl}_2$), and gypsum ($\text{CaSO}_4 \cdot 2\text{H}_2\text{O}$)) and 3 spectra acquired on point #1, #2 and #3. Sulfur fluorescence mappings, obtained at 2.4716, 2.4725, 2.4828 and 2.5000 keV. Map size: $60 \times 18 \mu\text{m}^2$, step size: 0.5 μm in both directions. Cf. visible picture in Fig. 3.

Consequently, four fluorescence mappings were acquired at four characteristic energies: 2.4716 keV, where cinnabar is over-excited, 2.4725 keV, where corderoite is over-excited, 2.4828 keV, where sulfates are over-excited, and at 2.5 keV, above the different edges, in order to get an image of the whole sulfur, whatever its speciation. The different raw maps are shown in Fig. 5. They clearly demonstrate the variation of the sulfur chemical environment across the stratigraphy. A simple ternary model was considered to treat mappings and calculate corresponding chemical images. This semi-quantitative approach consists of decomposing absorption as the sum of three components, these vectors being the reference spectra of cinnabar, corderoite and gypsum. The principle of this calculation is detailed elsewhere.¹⁰ Corresponding mappings are shown with RGB display in Fig. 6B. They clearly demonstrate the succession of strata: corderoite forms a superficial thin, grey layer on top of cinnabar grains, while sulfates are mostly present in the thick, translucent superficial film.

Contrary to a previous study where sulfates were found to be responsible for cinnabar blackening,¹⁰ here, their presence is more likely associated to the voluntary covering of the monastery wall with whitewash. Its complete removal was avoided to preserve the subjacent painted layer. This remaining micrometric superficial layer still partially covers walls, leaving a white film in places.

Beyond this sulfate layer, and on top of corderoite, a very thin sulfur-free layer can be noticed. This area corresponds to a high concentration of mercury chlorides (Fig. 4). The RGB map (Fig. 6C) compiles the different states of degradation of cinnabar: safe cinnabar in red, corderoite-like sulfur in green, and mercury chlorides in blue. It reveals a kind of chronology in

the “digestion” of cinnabar by chlorine: first from HgS to $\text{Hg}_3\text{S}_2\text{Cl}_2$, and then to sulfur-free mercury chlorides such as $(\text{HgCl})_2$ or HgCl_2 , $\text{Hg}_6\text{Cl}_3\text{O}(\text{OH})$ or Hg_2ClO , all these phases being responsible for the grey layer observed on red cinnabar.

Corderoite ($\text{Hg}_3\text{S}_2\text{Cl}_2$) is already known to be photosensitive and to degrade under the action of light, leading in particular to the formation of calomel ($(\text{HgCl})_2$).^{8,9} This work gives a clear image of the successive steps of the degradation mechanism.

Additional studies are ongoing to better understand the real effect of environmental parameters, such as light and oxygen on the process. In this case, the phenomenon clearly develops on top of the cinnabar grains. But it would be very interesting to determine to which extent chlorine is present behind cinnabar, as CaCl_2 , can be a danger for future alteration.

This analysis benefits from the high sensitivity of μXRF to detect traces of chlorine. Secondly, energy tunability and spatial resolution were crucial to generate chemical images. This method offers a unique direct observation of chemical reactions occurring on the surface of cinnabar grains. More generally, chlorine is often associated in various degradation mechanisms spreading on art objects and affecting not only cinnabar but also lead or copper pigments as well as other materials like metals. Lots of studies could benefit from a similar methodological approach, exceeding the simple elemental identification.

Combination of μFTIR , $\mu\text{XRD}/\mu\text{XRF}$ to identify Bamiyan Buddhist painting techniques

In the second example, the focus is made on the identification of practices used in Bamiyan Buddhist paintings. Bamiyan, Foladi and Kakrak sites are located in the highlands of Afghanistan, in the middle of Bamiyan valley, where Buddhism flourished between the 5th and 9th centuries. This period is symbolised by two Giant Buddhas, magnificent Buddhist paintings in caves, temples and possibly a nirvana Buddha. About 50 caves still keep some but very few remaining portions of the mural paintings are left after demolition by Taliban. The Bamiyan site was, therefore, inscribed in 2003 on the World Heritage Danger List, and became subject to protection within an international cooperation. Since this project has been funded by the UNESCO-Japanese Funds-in-Trust, a Japanese institution, NRICP, was chosen to execute the conservation project, ‘Safeguarding of the Bamiyan Site’ within the framework of UNESCO.²¹

Aiming to set appropriate conservation strategies and to comprehend the painting techniques of the Bamiyan Mural Paintings, detailed technical studies for painting materials and studies for deterioration mechanisms were developed. Although the paintings represent Buddhist patterns and stories, their painting materials and techniques could have been strongly influenced by Mediterranean or West Asian regions through trade in the ancient period. Chemical analyses are a good way to tackle any evidence of both organic and inorganic material influences from various regions in a broader context. Experiments were conducted at the ESRF on thin cross-sections of about 45 fragments by combining $\mu\text{XRD}/\mu\text{XRF}$ (ID18F) and μFTIR (ID21). One particular example (from Foladi cave 4: ca. 8th century AD) is given to illustrate the potential of the combination of these techniques. A larger overview of results and discussion will be given in a forthcoming article.

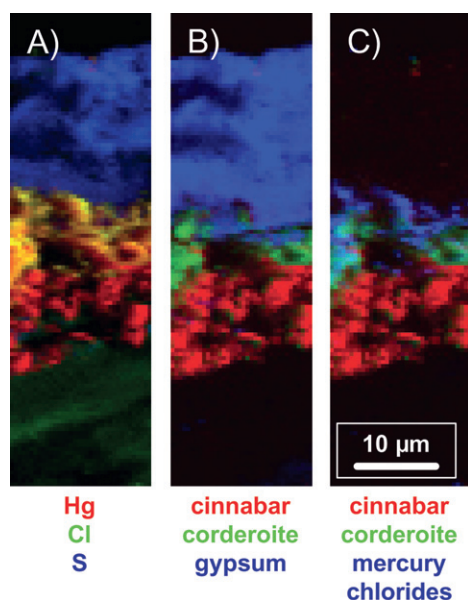


Fig. 6 Elemental and chemical mappings of the cinnabar blackening, with RGB visualization. Map size: $60 \times 18 \mu\text{m}^2$, step size: $0.5 \mu\text{m}$ in both directions. (A) Elemental distribution of Hg (red), Cl (green) and S (blue). (B) Chemical distribution of sulfur speciation decomposed on three vectors: cinnabar (red), corderoite (green) and gypsum (blue). (C) Summary of the different alteration products: cinnabar (red), corderoite (green) and mercury chlorides (blue). Cf. visible picture in Fig. 3.

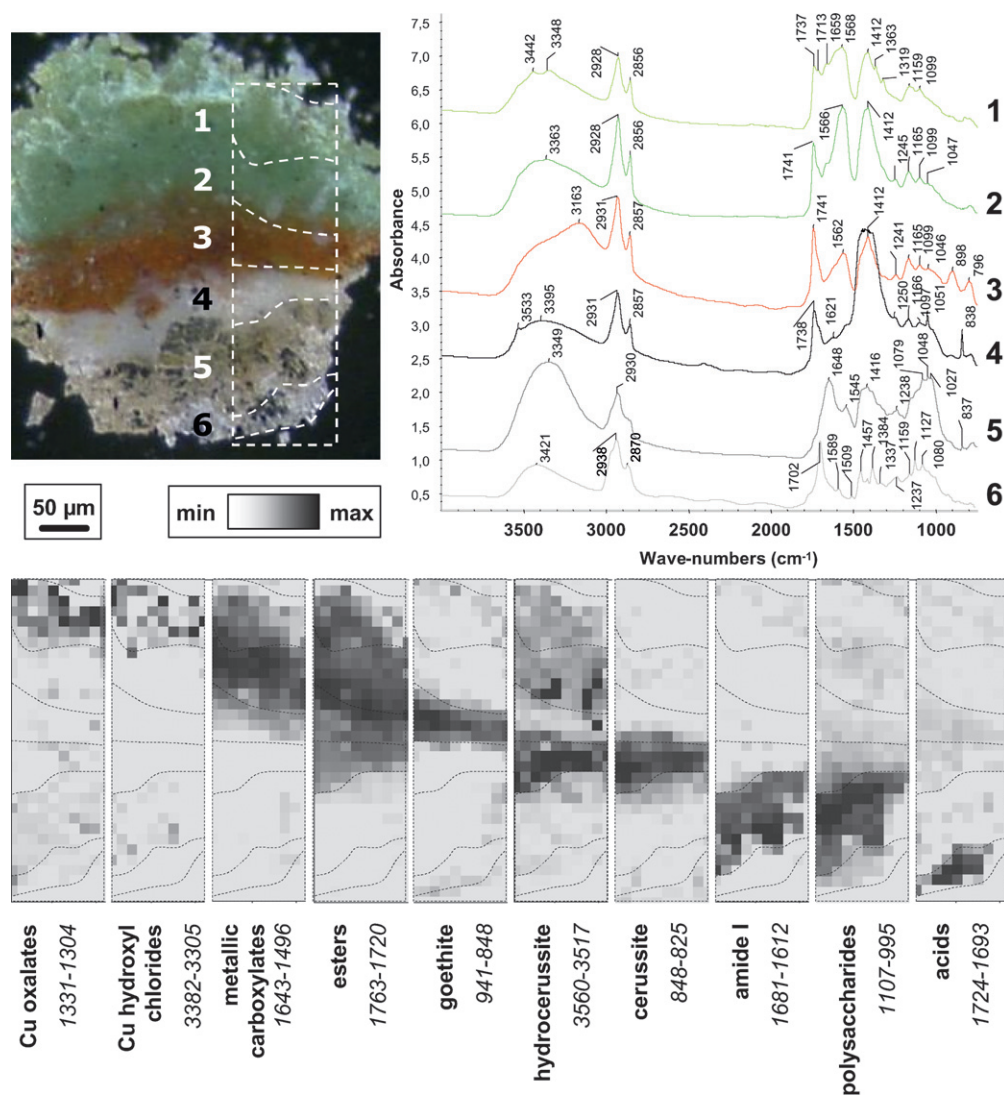


Fig. 7 μ FTIR analysis of a pressed painting fragment from Foladi. Visible light picture, average FTIR spectra and chemical mappings. Regions of interest considered to calculate maps are indicated in wave-numbers. Map size: $144 \times 384 \mu\text{m}^2$; step and beam size: $12 \times 12 \mu\text{m}^2$.

Fig. 7 shows a painting fragment after compression in diamond windows. Stratigraphy has been preserved with layers wider than before compression. Average FTIR spectra are calculated on the different coloured layers (indexed as follows, from surface to ground: 1: light green, 2: dark green, 3: red, 4: white, 5: translucent brown and 6: translucent white). The layers 1–3 are paint layers, and 4 is a ground layer, and the layers 5 and 6 are characterised as sizing layers which were applied on the earthen plaster render in order to provide a better surface for depicting the paintings. Similarities and differences can be observed. In spectra 1 to 4, C–H ($\nu_{\text{max}}/\text{cm}^{-1} \sim 2930$) and C=O ester ($\nu_{\text{max}}/\text{cm}^{-1} \sim 1740$) stretching modes support the identification of an oily binder. Hydrocerussite ($\text{Pb}_3(\text{CO}_3)_2(\text{OH})_2$), identified through the characteristics O–H stretching at $\nu_{\text{max}}/\text{cm}^{-1} 3533$, is concentrated in layer 4, and more diluted in layers 1 and 2. In layer 2, some high spots of hydrocerussite are observed, corresponding to white grains discernible on the visible picture. Cerussite (PbCO_3), usually associated to hydrocerussite in lead white,²² is almost concentrated in the white layer 4. In layer 1,

different copper compounds, such as copper oxalates (doublet $\nu_{\text{max}}/\text{cm}^{-1} 1363\text{--}1319$) and copper hydroxyl-chlorides (doublet $\nu_{\text{max}}/\text{cm}^{-1} 3442\text{--}3348$), are observed. The large C=O stretching band ($\nu_{\text{max}}/\text{cm}^{-1} \sim 1568$) is associated to metallic carboxylates. Considering its shape and position, a mixture of both copper and lead soaps is hypothesized. This blend is present in the two green layers (1 and 2). The upper layer with copper oxalates could be an alteration layer of the layer 2 due to ageing. In layer 3, the red colour is partially due to goethite (FeOOH), identified by the doublet $\nu_{\text{max}}/\text{cm}^{-1} 896\text{--}796$ and the large OH stretching around $\nu_{\text{max}}/\text{cm}^{-1} 3163$. Layer 5 contains a mixture of proteins (characteristic amide I band around $\nu_{\text{max}}/\text{cm}^{-1} 1650$) and polysaccharides (C–O stretching around $\nu_{\text{max}}/\text{cm}^{-1} 1050$). It lets assume the use of mucilage and/or protein-based material, such as hide glue or egg. The signal from layer 6, in particular C=O acid stretching ($\nu_{\text{max}}/\text{cm}^{-1} \sim 1702$), is typical of a natural resin (such as mastic). Characteristic vibration signals were used to draw the distribution of the different components, pigments and binders (Fig. 7).

In this example, spectral quality was essential to enable the differentiation of the various compounds, in particular in the C=O stretching domain. By choosing appropriate regions of interest, it was possible to distinguish ester, acid, amide, carboxylate, carbonate and oxalate groups.

Parallel analyses were conducted on similar fragments by μ XRD/ μ XRF. 2D-mappings were performed with the simultaneous acquisitions of a diffraction pattern (in transmission) and of a fluorescence spectrum (at 90° from the incoming beam, in the horizontal plane) at each pixel of a 2D-array (Fig. 2B). Fluorescence and diffraction data sets were simultaneously handled with PyMCA. There is a clear cross-fertilization by analysing concomitantly elemental and structural information provided by XRF and XRD, respectively. In Fig. 8, the scheme of the stratigraphy (green (1), white (2), red (3), white (4), brown (5) and light brown (6) layers) is superimposed to some elemental mappings (Cu, Cl, Pb, Fe and K). Average diffraction patterns were then calculated over the same identified areas (Fig. 9). The brown layer (6) mainly exhibits a quartz pattern. In the light brown ground layer (5), no minerals are detected. As seen by μ FTIR, hydrocerussite and cerussite are present in layers 1 to 4, with a varying ratio which can be estimated by comparing the intensity at $d = 2.622$ and 3.498 Å ($\theta = 4.843$ and 3.629°), characteristic of hydrocerussite and cerussite, respectively (Fig. 8 and Fig. 9). Copper compounds, pigments and altered products, suspected by μ FTIR, were identified more accurately, in green layer: hydroxyl chlorides (atacamite, $\text{Cu}_2\text{Cl}(\text{OH})_3$ and $\text{Cu}_7\text{Cl}_4(\text{OH})_{10}\cdot\text{H}_2\text{O}$) and moolooite ($\text{CuC}_2\text{O}_4\cdot n\text{H}_2\text{O}$). Traces of lead sulfates (palmierite, $(\text{K},\text{Na})_2\text{Pb}(\text{SO}_4)_2$ and anglesite, PbSO_4)

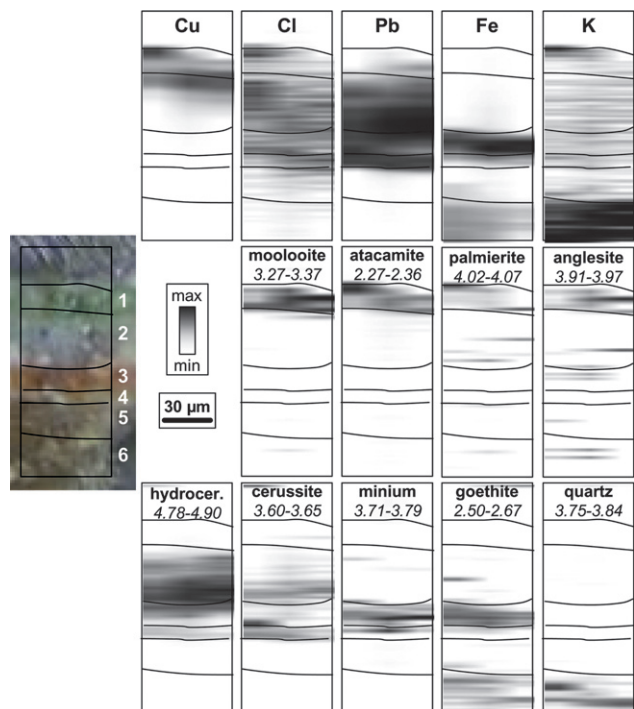


Fig. 8 μ XRF/ μ XRD analysis of a thin cross-section of a painting fragment from Foladi. Visible light picture, elemental and phase mappings. Regions of interest considered to calculate phase maps are indicated in degrees. Map size: $60 \times 150 \mu\text{m}^2$; step and beam size: $15 \times 1 \mu\text{m}^2$ (hor. \times ver.).

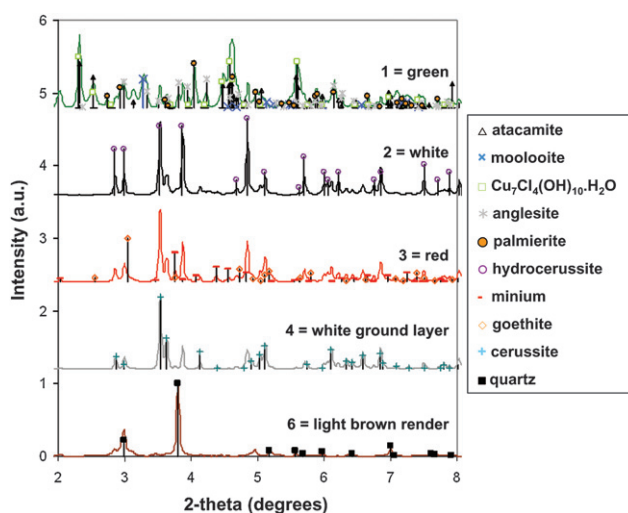


Fig. 9 Average diffraction patterns obtained on the different layers (*cf.* Fig. 4) and main reference patterns.

were detected on the painting surface. In the red layer, a small contribution of two pigments can be noticed: goethite ($\text{FeO}(\text{OH})$) but also minium (Pb_3O_4).

All these analyses reveal the presence of a broad range of compounds, with a high diversity not only of pigments but also of binders. The complete stratigraphy is sketched in the electronic supplementary information.† Original ingredients (minium, goethite, lead white *etc.*) and alteration compounds (oxalates and sulfates) are simultaneously identified. The varying proportions of these components are also indicative of complex painting techniques. This on-going project sheds a new light on artistic practices used 15 centuries ago, in Bamiyan, a cross-road between the East and the West through the Eurasia Continent, at the middle of the Silk Road. To our knowledge, some paintings after the mid 7th century AD of Bamiyan could be the first and therefore oldest examples of oil paintings on Earth, since there is a very limited number of analyses of Central Asian pictorial works of art so far. Lots of questions are still to be tackled, not only on the choice of ingredients but also on their use and combination. For example, do the metallic carboxylates result from a voluntary synthesis or from a long alteration with oil and minerals? What can explain the varying ratio of hydrocerussite and cerussite, these two lead carbonates being constitutive of lead white: voluntary choice of different quality of lead white? Different use of the same lead white, mixed with oil? Subsequent alteration? A more quantitative treatment of data will be necessary to answer these questions, to reveal all the secrets kept in these ancient complex paintings.

This example is illustrative of the interest of combining different micro-imaging techniques. μ FTIR is crucial for the identification of organic binders but also hybrid materials such as metallic carboxylates formed by interaction between organic matter and minerals. μ FTIR can also provide information about minerals even if μ XRD is the key method for the clear identification of these phases. In the present example, it was the only method susceptible to reveal the presence of minium (Pb_3O_4), which is transparent in the mid-IR spectral domain, and for which XRF analysis is made ambiguous by the presence of lead

carbonates. μ XRF is a good complement of both μ FTIR and μ XRD, as it will help the interpretation of data, thanks to elemental identification. In this example, the identification of palmierite $(\text{K},\text{Na})_2\text{Pb}(\text{SO}_4)_2$ is highly supported by its co-location to potassium on the surface of the sample, over the green layer.

The interests of micro-imaging are obvious in this case as the ingredients are not only identified but they are also located over the stratigraphy. The possibility to calculate average spectra or diffraction patterns over specific regions (for example red layer) is a clear asset for the data interpretation. This way, chemicals (for example minium) that would be an invisible trace at the scale of the whole sample, can be over-expressed locally, and thus identified. Lateral resolution is indeed crucial for the selective study of each coloured layer.

Conclusion

The unique properties of synchrotron radiation (e.g., high brightness, small probe and wavelength tunability) offer a very favourable context for the development of micro-analysis techniques. Imaging techniques appear to be an important analytical tool for the study of structured and heterogeneous arrangements as occurring in paintings. Micrometre probes are essential for the discriminative study of each layer. μ FTIR is particularly useful for the detection and location of the different organic binders (fat, protein, resin *etc.*) μ XRD is more adapted for the accurate identification of mineral compounds. Combined with μ XRF, it offers a powerful tool for the precise analysis of pigments, plasters and alteration products. The major advantage of μ XANES is the possibility to specifically study the chemical environment of a particular element, even diluted in a complex mixture. Finally, in addition to the common and distinct advantages of the different synchrotron based-techniques, the combination of all these micro-analytical tools provides a unique integrated approach for the chemical analysis of art objects in general, and paintings in particular.

Although access to synchrotron instruments is intrinsically limited, the methods developed can have a broader impact if they can migrate and be adapted to the laboratory. Indeed, the development of new methodologies would greatly benefit from a better synergy between synchrotron and laboratory teams. It led, for example, to the development of common platform and versatile analytical software packages.

Acknowledgements

This study was funded by grants from ESRF (Project EC-101 and In-House Research). The authors thank the restorers team, Josep M^a Julià and Alicia Calmell (Servei d'Arquitectura,

Ajuntament de Barcelona), the Institut del Paisatge Urbà (Barcelona), Anna Castellano from the Museu-Monestir de Pedralbes and Closa-Alegret S.A for the access to Pedralbes paintings. They are grateful to the Ministry of Information and Culture of Afghanistan and UNESCO for their kind assistance.

A part of this study has been funded by the Grant-in-Aid for Scientific Research [18700680], Grant-in-Aid for Young Scientists (B) from the Ministry of Education, Culture, Sports, Science and Technology of Japan. The authors thank the referees for their prompt and thorough reading of the manuscript.

References

- 1 K. Janssens, in *Comprehensive Analytical Chemistry*, XLII, ed. K. Janssens and R. Van Grieken, Elsevier, Amsterdam, 2004, ch. 4.
- 2 S. Bruni, F. Cariati, F. Casadio and L. Toniolo, *Vib. Spectrosc.*, 1999, **20**, 15–25.
- 3 D. Hradil, T. Grygar, J. Hradilova, P. Bezdieka, V. Grunwaldova, I. Fogas and C. Miliani, *J. Cult. Herit.*, 2007, **8**, 377–386.
- 4 M. E. Laver, in *Artists' Pigments: A Handbook of their History and Characteristics*, ed. Elizabeth West FitzHugh, National Gallery of Art, Washington, 1997, vol. 3, pp. 295–339.
- 5 H. G. M. Edwards and N. F. N. Hassan, *Anal. Bioanal. Chem.*, 2006, **384**, 1356–1365.
- 6 K. Keune, PhD thesis, University of Amsterdam, 2005.
- 7 See for example <http://srs.dl.ac.uk/arch/>.
- 8 M. Spring and R. Grout, *Natl. Gallery Technol. Bull.*, 2002, **23**, 50–61.
- 9 K. Keune and J. J. Boon, *Anal. Chem.*, 2005, **77**, 4742–4750.
- 10 M. Cotte, J. Susini, A. Moscato, C. Gratzu, A. Bertagnini and N. Metrich, *Anal. Chem.*, 2006, **78**, 7484–7492.
- 11 N. Wyplosz, R. Koper, J. van der Weerd, R. Heeren and J. J. Boon, *Art et Chimie la Couleur, proceedings*, ed. J. Goupy and J. P. Mohen, CNRS edition, Paris, 2000, pp. 65–68.
- 12 J. Boon and S. Asahina, *Microsc. Microanal.*, 2006, **12**(Supp 2), 1322.
- 13 V. Mazel, P. Richardin, D. Debois, D. Touboul, M. Cotte, A. Brunelle, P. Walter and O. Laprévote, *Anal. Chem.*, 2007, **79**, 9253–9260.
- 14 J. Susini, M. Salomé, B. Fayard, R. Ortega and B. Kaulich, *Surf. Rev. Lett.*, 2002, **9**, 203–211.
- 15 M. Cotte, E. Welcomme, V. A. Solé, M. Salomé, M. Menu, Ph. Walter and J. Susini, *Anal. Chem.*, 2007, **79**, 6988–6994.
- 16 A. Somogyi, M. Drakopoulos, L. Vincze, B. Vekemans, C. Camerani, K. Janssens, A. Snigirev and F. Adams, *X-Ray Spectrom.*, 2001, **30**, 242–252.
- 17 J. Susini, M. Cotte, K. Scheidt, O. Chubar, F. Polack and P. Dumas, *Synchrotron Radiat. News*, 2007, **20**(5), 13–16.
- 18 V. A. Solé, E. Papillon, M. Cotte, Ph. Walter and J. Susini, *Spectrochim. Acta, Part B*, 2007, **62**(1), 63–68.
- 19 A. P. Hammersley and C. Riekel, *Synchrotron Radiat. News*, 1989, **2**, 24–26.
- 20 R. J. Gettens, R. L. Feller and W. T. Chase, *Stud. Conserv.*, 1972, **17**, 45–69.
- 21 Japan Center for International Cooperation in Conservation report, *Protecting the World Heritage Site of Bamiyan: Key Issues for the Establishment of a Comprehensive Management Plan*, National Research Institute for Cultural Properties, Tokyo, Japan, 2004.
- 22 E. Welcomme, Ph. Walter, P. Bleuët, J.-L. Hodeau, E. Dooryhee, P. Martinetto and M. Menu, *Appl. Phys. A: Mater. Sci. Process.*, 2007, **89**(4), 825–832.